J. Phys. B: At. Mol. Opt. Phys. **33** (2000) 1013–1028. Printed in the UK PII: S0953-4075(00)06913-3

Electron-impact excitation of C^{3+} and O^{5+}: the effects of coupling to the target continuum states

D C Griffin†, N R Badnell‡ and M S Pindzola§

† Department of Physics, Rollins College, Winter Park, FL 32789, USA
‡ Department of Physics and Applied Physics, University of Strathclyde, Glasgow G4 0NG, UK
§ Department of Physics, Auburn University, Auburn, AL 36849, USA

Received 12 August 1999, in final form 6 December 1999

Abstract. We have carried out extensive *R*-matrix close-coupling calculations of the electron-impact excitation of C^{3+} and O^{5+}. We have determined effective collision strengths for transitions between the lowest nine terms and cross sections between the ground state and selected excited terms of these ions from 41-state *R*-matrix with pseudo-states (RMPS) calculations that employ basis sets consisting of nine physical states and 32 pseudo-states. In order to investigate the dependence of electron-impact excitation on coupling of the bound states to the target continuum states and also the highly excited bound states included in these RMPS calculations, we have compared these results with those determined from our 9-state and 13-state *R*-matrix calculations without pseudo-states. As one would expect, this additional coupling is in general less important in O^{5+} than in C^{3+}; however, these effects vary significantly with the type of transition and are complicated by the resonance contributions. This makes it difficult to draw any general conclusions regarding their dependence on ionization stage. These results complement earlier work on the Li-like ions Be^+ and B^{2+} and provide improved sets of excitation data for these ions.

1. Introduction

In recent years, much progress has been made on the development of advanced time-independent close-coupling methods that are capable of accurately treating the target continuum. In particular, the convergent close-coupling (CCC) method [1], and the *R*-matrix with pseudo-states (RMPS) method [2] have been successfully applied to the study of electron-impact excitation and ionization in a variety of atomic targets. With respect to electron-impact excitation, these techniques allow one to include the effects of coupling of the bound states to the continuum (and to the highly excited bound states). For example, these effects have been investigated in the Li-like ions Be^+ by Bartschat and Bray [3] and B^{2+} by Marchalant *et al* [4], using the CCC and the *R*-matrix with RMPS methods. By comparing the results of CCC and RMPS calculations for these Li-like ions with 9-state *R*-matrix close-coupling calculations without pseudo-states, they explored the importance of coupling to the continuum on the electron-impact excitation cross sections from the ground state. As one might expect, they found that this additional coupling had very small effects on the $2s \rightarrow 2p$ excitation, but pronounced effects on many of the $2s \rightarrow 3\ell$ and $2s \rightarrow 4\ell$ excitations. Although it appears that these effects are somewhat reduced in B^{2+}, as compared with Be^+, they are still quite pronounced in this doubly ionized species.

A more systematic study of coupling to highly excited bound and continuum states as a function of ionization stage was carried out on the $ns \rightarrow n's$ excitations in the H-like ions

0953-4075/00/051013+16$30.00

He^+, Li^{2+}, Be^{3+} and B^{4+} by Badnell and Gorczyca [5]. By comparing the results of RMPS calculations with *R*-matrix calculations without pseudo-states, they were able to show that these extra coupling effects fall off approximately as $1/z$ for these transitions, where z is the charge on the target ion.

Electron-impact excitation of carbon and oxygen ions is of importance to both astrophysical and laboratory plasma research. Burke has performed a 9-state *R*-matrix close-coupling calculation of the effective collision strengths between the lowest nine terms of C^{3+} [6]. Fisher *et al* [7] have employed the CCC and the Coulomb–Born with exchange and normalization methods to generate fits to the cross sections between the lowest nine terms in the Li-like ions. Their fitting formulae allow one to generate cross sections for any of the Li-like ions from C^{3+} on up the isoelectronic sequence. However, their CCC calculations did not include the continuum in the pseudo-state expansion, and therefore, these results do not include the effects of coupling to the target continuum. There has also been a recent RMPS calculation of the 2s $\rightarrow$ 2p excitation in C^{3+} in order to compare with measurements of this cross section [8].

In a recent paper, we applied the RMPS method to the ionization of C^{3+} [9]. In that study, we performed a series of calculations in which we increased the size of the pseudo-state basis set in order to investigate the convergence of the RMPS method with the angular momentum of the target continuum. We discovered that ionization cross sections from our 41-state RMPS calculation that included s-, p-, d- and f-electron pseudo-states was in excellent agreement with our 62-state RMPS calculation (that also included both g- and h-electron pseudo-states) at energies below the peak in the ionization cross section and differed from the 62-state cross sections by only about 5% for energies above the peak in the cross section. Thus the 41-state RMPS basis set appears sufficiently converged with respect to the size of the pseudo-state expansion to provide an excellent test of the effects of continuum coupling on the excitation cross sections in C^{3+} and O^{5+}. This 41-state expansion is larger than the pseudo-state expansions employed in the studies of coupling effects in Be^+ [3] and B^{2+} [4], but is similar to those expansions in that it includes only s-, p-, d- and f-electron pseudo-states.

In this paper, we present the results of our 41-state RMPS calculations of electron-impact excitation between the lowest nine terms in C^{3+} and O^{5+} in comparison to the results of both 13-state and 9-state *R*-matrix calculations without pseudo-states. In this way, we are able to study the effects of coupling of the bound states to the target continuum states, and also the highly excited bound states, in these two ions. Our RMPS results should also provide improved effective collision strengths for use in collisional–radiative modelling for these ions.

The remainder of this paper is organized as follows. In section 2, we discuss the computational details regarding our non-pseudo-state *R*-matrix and RMPS calculations. In section 3, we present and compare the results of our calculations of effective collision strengths for C^{3+} and O^{5+}. In addition, we compare our calculated cross sections for the 2s $\rightarrow$ 2p excitation in the threshold region with experimental measurements and other calculations. Finally, we compare our excitation cross sections with each other and with cross sections calculated from the fitting formula of Fisher *et al* [7] for the 2s $\rightarrow$ 2p and several other transitions in these ions. In section 4, we summarize our findings and discuss their implications.

2. Description of theoretical calculations

Because prior RMPS and CCC calculations were compared to 9-state *R*-matrix calculations in Be^+ and B^{2+} [3, 4], we began our work on C^{3+} and O^{5+} by performing both RMPS and non-pseudo-state 9-state *R*-matrix calculations. However, we also performed 13-state calculations that included the additional four terms arising from the 5s, 5p, 5d and 5f configuration; as we

shall see, by comparing these 13-state calculations with the 9-state and RMPS calculations, we can attempt to distinguish between the effects of coupling to highly excited bound and continuum states and the effects of resonances attached to bound states with $n \geqslant 5$. For our 9-state R-matrix calculations and our 41-state RMPS calculations, we first calculated 1s, 2s, 2p, 3s, 3p, 3d, 4s, 4p, 4d and 4f physical orbitals using Froese Fischer's Hartree–Fock (HF) programs [10]. These bound HF spectroscopic orbitals are then similar to those bound HF orbitals employed in Be^+ and B^{2+} [3, 4]. For our 13-state non-pseudo-state R-matrix calculations, we also calculated the 5s, 5p, 5d and 5f HF orbitals. We then generated a set of non-orthogonal Laguerre orbitals of the form

$$P_{n\ell}(r) = N_{n\ell}(\lambda_\ell Zr)^{\ell+1}\mathrm{e}^{-\lambda_\ell Zr/2}L_{n+\ell}^{2\ell+1}(\lambda_\ell Zr), \tag{1}$$

using the program AUTOSTRUCTURE [11]. In this equation, $L_{n+\ell}^{2\ell+1}(\lambda_\ell Zr)$ denotes the associated Laguerre polynomial; $N_{n\ell}$ is a normalization constant; and $Z = z+1$, where z is the residual charge on the ion. These Laguerre orbitals are then orthogonalized to the HF orbitals and to each other. The scaling parameters λ_ℓ allow one to adjust the energy of the pseudo-states, determined from a configuration-interaction (CI) expansion of the pseudo-orbitals, as well as the radial extent of the pseudo-orbitals.

In the 9-state and 13-state calculations, only the physical orbitals were employed to represent the target. However, for the 41-state RMPS calculations, we employed the 10 physical orbitals that were used in the 9-state calculation plus the 32 pseudo-orbitals from 5s, 5p, 5d and 5f up to 12s, 12p, 12d and 12f, giving rise to a 41-term CI expansion of the target. However, by Brillouin's theorem [12], there can be no mixing among the physical orbitals, or between the physical orbitals and the pseudo-orbitals, since the physical orbitals were determined from HF calculations on each individual $1s^2n\ell\ ^2\mathrm{L}$ term. Thus, the nine physical terms in the 41-state calculation are the same single-configuration HF states used in the 9-state R-matrix and the first nine terms used in the 13-state R-matrix calculation, while the 32 pseudo-states within the 41-state calculation are formed from expansions that include only pseudo-orbitals of a given symmetry. This provides the added advantage that the differences between electron-impact excitation cross sections among the nine lowest terms, as calculated from these target representations, are solely due to added coupling effects and added resonance contributions, and are not affected by differences in the CI expansions of the target.

In these calculations, we used the same procedure to determine the screening parameters, λ_ℓ, as we employed in our ionization calculations for C^{3+} [9]. Namely, we adjusted them until the ionization limit was roughly midway between two term energies of the same symmetry. For both C^{3+} and O^{5+}, the scaling parameters determined in this way were: $\lambda_{ns} = 0.90$, $\lambda_{np} = 0.88$, $\lambda_{nd} = 0.90$ and $\lambda_{nf} = 0.96$. This procedure for determining the values of λ_ℓ enhances the accuracy of ionization calculations; however, as we shall see, it also provides a reasonably good representation of the highly excited bound states by the set of pseudo-orbitals. With our set of screening parameters, the $n = 5$ and $n = 6$ pseudo-states are bound, while those with $n \geqslant 7$, lie above the ionization limit. Furthermore, the 5ℓ and 6ℓ pseudo-states are in spectroscopic order by ℓ, while the pseudo-states above the ionization limit are not. We will discuss the nature of these bound pseudo-states in more detail in the next section.

The R-matrix calculations with exchange were performed in LS coupling using a modified version of the RMATRX I package [13]. The box orbitals used to represent the $(N+1)$-electron continuum were made orthogonal to the pseudo-orbitals using a method developed by Gorczyca and Badnell [14]. For the 9-state and 41-state calculations in C^{3+}, we employed 40 continuum basis orbitals per angular momentum; the 9-state calculation required an R-matrix box of radius 18.0 au, while the 41-state calculation required a box of radius 20.8 au. For the 13-state calculation in C^{3+}, we used 55 continuum basis orbitals per angular momentum and it required

an R-matrix box of 26.7 au. For the 9-state and 41-state calculations in O^{5+}, we employed 38 continuum basis orbitals per angular momentum; the 9-state calculation required an R-matrix box of radius 12.0 au and the 41-state calculation required a box of radius 14.0 au. For the 13-state R-matrix calculation in O^{5+}, we used 48 continuum basis orbitals per angular momentum and it required an R-matrix box of 17.2 au.

All $LS\Pi$ symmetries up to $L = 12$ were included in these calculations. However, for the determination of effective collision strengths between the lowest nine terms of these ions, $L = 12$ is not nearly high enough to ensure convergence of the partial-wave sum. Thus, we also performed no-exchange R-matrix calculations for all $LS\Pi$ partial waves from $L = 13$ to $L = 60$. These were then topped up using methods described in Badnell *et al* [15] and added to the results of the exchange calculation. In order to resolve narrow resonance structures in C^{3+}, we employed an energy mesh of 2.15×10^{-4} z^2-scaled Rydbergs up through the energy of the $n = 6$ pseudo-states, where z is the charge of the ion; for the higher energies, we employed an energy mesh of 1.35×10^{-2} z^2-scaled Rydbergs. In O^{5+}, energy meshes of 1.15×10^{-4} z^2-scaled Rydbergs and 9.60×10^{-3} z^2-scaled Rydbergs were employed.

3. Results

The effective collision strength, Υ, first introduced by Seaton [16] is defined by the equation

$$\Upsilon_{ij} = \int_0^\infty \Omega(i \rightarrow j) \exp\left(\frac{-\epsilon_j}{kT_e}\right) \mathrm{d}\left(\frac{\epsilon_j}{kT_e}\right), \tag{2}$$

where Ω is the collision strength for the transition from level i to level j and ϵ_j is the continuum energy of the final scattered electron. Effective collision strengths have a much more gradual variation with temperature than rate coefficients and are, therefore, much better suited for interpolation over temperature.

Our calculated effective collision strengths between the nine lowest terms in C^{3+} and O^{5+}, obtained from our 41-state RMPS calculations, our 13-state R-matrix calculations without pseudo-states and our 9-state R-matrix calculations without pseudo-states, are given in that order in three rows for each transition in tables 1 and 2 and tables 3 and 4, repectively. Our 9-state results for C^{3+} that are shown in the last row for each transition in tables 1 and 2 are in good agreement with the earlier results of Burke [6]. The average percentage difference between the effective collision strengths calculated from these two 9-state calculations for all transitions and temperatures given in tables 1 and 2 is 4.7%. Furthermore, the percentage differences between the effective collision strengths from these two calculations, averaged over the six temperatures in tables 1 and 2 (temperature-averaged percentage differences) for each transition, are all less than 11%. This level of agreement seems quite reasonable in light of differences between these two 9-state calculations with respect to: (1) the bound-state radial orbitals, (2) the number of continuum box states of each symmetry used to represent the $(N + 1)$-electron continuum and (3) the energy meshes employed in the low-energy region.

We first focus on the $2s \rightarrow 2p$ transition. For C^{3+}, the differences between the 9-state and 13-state effective collision strengths given in the second and third rows of table 1 are negligible and the RMPS effective collision strengths given in the first row of table 1 differ from the two non-pseudo-state R-matrix results by about only 1% for all temperatures. In figure 1, we show the cross sections for this transition in C^{3+} in the threshold region; we compare the cross sections from our three calculations with the RMPS calculation for this transition reported in the paper by Janzen *et al* [8] and various experimental measurements. In (*a*), the theoretical cross sections are convoluted with a 1.74 eV Gaussian, which is the electron-energy spread for the measurements of Janzen *et al* [8]; also shown in (*a*) are the measurements of Taylor

Table 1. Effective collision strengths for the first 18 transitions between the lowest nine terms of C^{3+}. For each transition, the first row is from the present 41-state pseudo-state calculation, the second row is from the present 13-state calculation and the third row is from present the 9-state calculation.

	Electron temperature (K)					
Transition	2.25×10^4	4.50×10^4	9.00×10^4	1.35×10^5	1.80×10^5	3.60×10^5
2s–2p	8.69×10^0	9.00×10^0	9.55×10^0	9.99×10^0	1.04×10^1	1.16×10^1
	8.76×10^0	9.08×10^0	9.63×10^0	1.01×10^1	1.05×10^1	1.17×10^1
	8.78×10^0	9.09×10^0	9.65×10^0	1.01×10^1	1.05×10^1	1.17×10^1
2s–3s	5.21×10^{-1}	4.51×10^{-1}	3.91×10^{-1}	3.66×10^{-1}	3.54×10^{-1}	3.44×10^{-1}
	5.70×10^{-1}	4.89×10^{-1}	4.25×10^{-1}	4.00×10^{-1}	3.89×10^{-1}	3.83×10^{-1}
	5.85×10^{-1}	5.06×10^{-1}	4.43×10^{-1}	4.17×10^{-1}	4.06×10^{-1}	3.98×10^{-1}
2s–3p	3.09×10^{-1}	2.78×10^{-1}	2.50×10^{-1}	2.36×10^{-1}	2.33×10^{-1}	2.43×10^{-1}
	3.13×10^{-1}	2.88×10^{-1}	2.62×10^{-1}	2.49×10^{-1}	2.45×10^{-1}	2.55×10^{-1}
	3.22×10^{-1}	2.99×10^{-1}	2.75×10^{-1}	2.62×10^{-1}	2.58×10^{-1}	2.64×10^{-1}
2s–3d	4.57×10^{-1}	4.66×10^{-1}	4.70×10^{-1}	4.74×10^{-1}	4.84×10^{-1}	5.37×10^{-1}
	4.89×10^{-1}	5.03×10^{-1}	5.12×10^{-1}	5.22×10^{-1}	5.39×10^{-1}	6.06×10^{-1}
	5.02×10^{-1}	5.22×10^{-1}	5.41×10^{-1}	5.54×10^{-1}	5.72×10^{-1}	6.37×10^{-1}
2s–4s	9.34×10^{-2}	7.75×10^{-2}	6.62×10^{-2}	6.25×10^{-2}	6.12×10^{-2}	6.10×10^{-2}
	1.11×10^{-1}	9.64×10^{-2}	8.52×10^{-2}	8.14×10^{-2}	8.02×10^{-2}	7.99×10^{-2}
	1.19×10^{-1}	1.04×10^{-1}	9.23×10^{-2}	8.85×10^{-2}	8.71×10^{-2}	8.61×10^{-2}
2s–4p	9.42×10^{-2}	8.57×10^{-2}	7.60×10^{-2}	7.20×10^{-2}	7.08×10^{-2}	7.24×10^{-2}
	1.13×10^{-1}	1.06×10^{-1}	9.55×10^{-2}	9.15×10^{-2}	9.04×10^{-2}	9.17×10^{-2}
	1.38×10^{-1}	1.27×10^{-1}	1.17×10^{-1}	1.13×10^{-1}	1.11×10^{-1}	1.10×10^{-1}
2s–4d	9.18×10^{-2}	9.06×10^{-2}	8.68×10^{-2}	8.65×10^{-2}	8.80×10^{-2}	9.63×10^{-2}
	1.31×10^{-1}	1.31×10^{-1}	1.28×10^{-1}	1.30×10^{-1}	1.33×10^{-1}	1.43×10^{-1}
	1.33×10^{-1}	1.37×10^{-1}	1.40×10^{-1}	1.45×10^{-1}	1.49×10^{-1}	1.59×10^{-1}
2s–4f	7.42×10^{-2}	7.01×10^{-2}	6.29×10^{-2}	5.96×10^{-2}	5.82×10^{-2}	5.71×10^{-2}
	9.74×10^{-2}	9.28×10^{-2}	8.32×10^{-2}	7.84×10^{-2}	7.58×10^{-2}	7.08×10^{-2}
	8.59×10^{-2}	8.20×10^{-2}	7.66×10^{-2}	7.40×10^{-2}	7.26×10^{-2}	6.93×10^{-2}
2p–3s	1.59×10^0	1.14×10^0	7.90×10^{-1}	6.40×10^{-1}	5.60×10^{-1}	4.45×10^{-1}
	1.73×10^0	1.22×10^0	8.38×10^{-1}	6.78×10^{-1}	5.93×10^{-1}	4.68×10^{-1}
	1.78×10^0	1.26×10^0	8.66×10^{-1}	7.02×10^{-1}	6.15×10^{-1}	4.83×10^{-1}
2p–3p	2.43×10^0	2.08×10^0	1.80×10^0	1.67×10^0	1.59×10^0	1.49×10^0
	2.37×10^0	2.13×10^0	1.92×10^0	1.81×10^0	1.75×10^0	1.69×10^0
	2.50×10^0	2.25×10^0	2.03×10^0	1.92×10^0	1.85×10^0	1.77×10^0
2p–3d	4.16×10^0	4.27×10^0	4.36×10^0	4.47×10^0	4.66×10^0	5.44×10^0
	4.34×10^0	4.49×10^0	4.63×10^0	4.79×10^0	5.02×10^0	5.92×10^0
	4.44×10^0	4.62×10^0	4.82×10^0	5.00×10^0	5.24×10^0	6.13×10^0
2p–4s	2.79×10^{-1}	2.03×10^{-1}	1.48×10^{-1}	1.25×10^{-1}	1.13×10^{-1}	9.18×10^{-2}
	2.85×10^{-1}	2.25×10^{-1}	1.75×10^{-1}	1.51×10^{-1}	1.38×10^{-1}	1.13×10^{-1}
	3.40×10^{-1}	2.59×10^{-1}	1.98×10^{-1}	1.71×10^{-1}	1.55×10^{-1}	1.25×10^{-1}
2p–4p	5.59×10^{-1}	4.82×10^{-1}	4.07×10^{-1}	3.72×10^{-1}	3.52×10^{-1}	3.19×10^{-1}
	6.63×10^{-1}	5.97×10^{-1}	5.22×10^{-1}	4.86×10^{-1}	4.66×10^{-1}	4.27×10^{-1}
	7.48×10^{-1}	6.67×10^{-1}	5.90×10^{-1}	5.51×10^{-1}	5.28×10^{-1}	4.77×10^{-1}
2p–4d	7.36×10^{-1}	7.40×10^{-1}	7.37×10^{-1}	7.58×10^{-1}	7.92×10^{-1}	9.24×10^{-1}
	9.47×10^{-1}	9.71×10^{-1}	9.95×10^{-1}	1.04×10^0	1.09×10^0	1.24×10^0
	1.04×10^0	1.08×10^0	1.13×10^0	1.18×10^0	1.23×10^0	1.37×10^0
2p–4f	4.69×10^{-1}	4.43×10^{-1}	3.92×10^{-1}	3.67×10^{-1}	3.54×10^{-1}	3.40×10^{-1}
	5.79×10^{-1}	5.50×10^{-1}	4.87×10^{-1}	4.53×10^{-1}	4.33×10^{-1}	3.98×10^{-1}
	5.11×10^{-1}	4.79×10^{-1}	4.35×10^{-1}	4.13×10^{-1}	4.00×10^{-1}	3.76×10^{-1}

Table 1. (Continued)

	Electron temperature (K)					
Transition	2.25×10^4	4.50×10^4	9.00×10^4	1.35×10^5	1.80×10^5	3.60×10^5
3s–3p	5.00×10^1	5.32×10^1	5.87×10^1	6.33×10^1	6.76×10^1	8.07×10^1
	4.78×10^1	5.17×10^1	5.75×10^1	6.22×10^1	6.67×10^1	8.04×10^1
	4.76×10^1	5.17×10^1	5.77×10^1	6.25×10^1	6.71×10^1	8.08×10^1
3s–3d	7.78×10^0	7.76×10^0	7.41×10^0	7.11×10^0	6.93×10^0	6.66×10^0
	7.86×10^0	7.83×10^0	7.48×10^0	7.21×10^0	7.06×10^0	6.84×10^0
	8.00×10^0	8.02×10^0	7.72×10^0	7.46×10^0	7.30×10^0	7.04×10^0
3s–4s	2.01×10^0	1.70×10^0	1.53×10^0	1.50×10^0	1.51×10^0	1.60×10^0
	1.89×10^0	1.70×10^0	1.59×10^0	1.60×10^0	1.63×10^0	1.77×10^0
	2.23×10^0	2.00×10^0	1.87×10^0	1.87×10^0	1.90×10^0	2.00×10^0

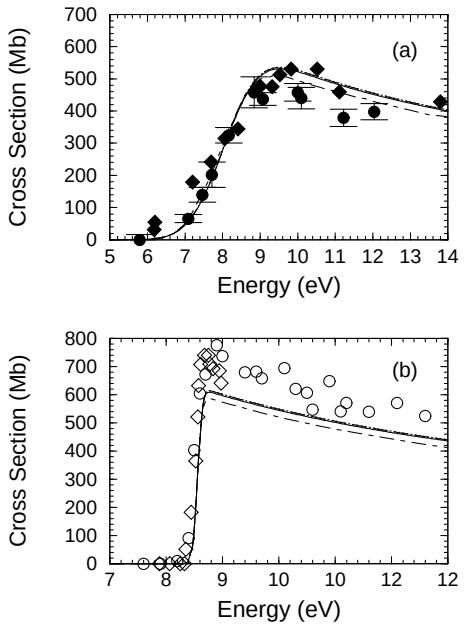

Figure 1. Electron-impact excitation cross sections for the 2s → 2p transition in C^{3+} in the threshold region. The dotted, dashed and solid curves (nearly indistinguishable in the graphs) are from the present 9-state non-pseudo-state *R*-matrix calculation, the present 13-state non-pseudo-state *R*-matrix calculation and the present 41-state RMPS calculation, respectively, which in (*a*) are convoluted with a 1.74 eV Gaussian and in (*b*) are convoluted with a 0.17 eV Gaussian; the dot-dashed curves are from the RMPS calculation reported in Janzen *et al* [8] which in (*a*) is convoluted with a 1.74 eV Gaussian and in (*b*) is convoluted with a 0.17 eV Gaussian; the solid circles are the measurements of Janzen *et al* [8]; the solid diamonds are the measurements of Taylor *et al* [17] the open circles are the measurements of Greenwood *et al* [19]; and the open diamonds are the measurements of Bannister *et al* [18].

et al [17], for which the electron-energy spread is actually 2.3 eV. In (*b*), the theoretical cross sections are convoluted with a 0.17 eV Gaussian, which is the electron-energy spread for the measurements of Bannister *et al* [18] and Greenwood *et al* [19]. The cross section from the 9-state *R*-matrix calculation of Burke [6] for this transition is indistinguishable from the cross section determined from our 9-state *R*-matrix calculation on the scale of these graphs. However, as can be seen, the RMPS results reported in Janzen *et al* [8] are below our three calculated cross sections. The level of agreement for the 2s → 2p cross section in C^{3+} between the 9-state *R*-matrix calculations and our RMPS calculation appears to be more consistent with the agreement between the 9-state *R*-matrix calculations and the RMPS calculations for the 2s → 2p excitation in Be^+ [3] and B^{2+} [4]. Thus, we are unable to explain the difference between these two RMPS calculations for the 2s → 2p transition in C^{3+}.

As one would expect, the agreement between the three sets of collision strengths for the 2s → 2p transition in O^{5+} shown in the first three rows of table 3 is slightly better than that of C^{3+}. In figure 2, we show the 2s → 2p cross sections for both C^{3+} and O^{5+} resulting from

Table 2. Effective collision strengths for the last 18 transitions between the lowest nine terms of C^{3+}. For each transition, the first row is from the present 41-state pseudo-state calculation, the second row is from the present 13-state calculation and the third row is from the present 9-state calculation.

	Electron temperature (K)					
Transition	2.25×10^4	4.50×10^4	9.00×10^4	1.35×10^5	1.80×10^5	3.60×10^5
3s–4p	7.74×10^{-1}	7.02×10^{-1}	6.50×10^{-1}	6.56×10^{-1}	6.91×10^{-1}	8.65×10^{-1}
	8.77×10^{-1}	7.87×10^{-1}	7.18×10^{-1}	7.16×10^{-1}	7.46×10^{-1}	9.08×10^{-1}
	8.27×10^{-1}	7.54×10^{-1}	7.17×10^{-1}	7.29×10^{-1}	7.65×10^{-1}	9.26×10^{-1}
3s–4d	1.25×10^{0}	1.28×10^{0}	1.33×10^{0}	1.41×10^{0}	1.49×10^{0}	1.76×10^{0}
	1.43×10^{0}	1.43×10^{0}	1.45×10^{0}	1.52×10^{0}	1.59×10^{0}	1.83×10^{0}
	1.31×10^{0}	1.35×10^{0}	1.43×10^{0}	1.52×10^{0}	1.61×10^{0}	1.86×10^{0}
3s–4f	1.78×10^{0}	1.79×10^{0}	1.78×10^{0}	1.82×10^{0}	1.87×10^{0}	2.01×10^{0}
	2.01×10^{0}	2.04×10^{0}	2.05×10^{0}	2.09×10^{0}	2.13×10^{0}	2.23×10^{0}
	2.17×10^{0}	2.19×10^{0}	2.19×10^{0}	2.22×10^{0}	2.25×10^{0}	2.31×10^{0}
3p–3d	1.24×10^{2}	1.31×10^{2}	1.41×10^{2}	1.49×10^{2}	1.57×10^{2}	1.84×10^{2}
	1.26×10^{2}	1.37×10^{2}	1.49×10^{2}	1.58×10^{2}	1.66×10^{2}	1.91×10^{2}
	1.27×10^{2}	1.38×10^{2}	1.50×10^{2}	1.59×10^{2}	1.67×10^{2}	1.92×10^{2}
3p–4s	3.82×10^{0}	2.61×10^{0}	1.93×10^{0}	1.76×10^{0}	1.75×10^{0}	2.03×10^{0}
	3.08×10^{0}	2.25×10^{0}	1.78×10^{0}	1.69×10^{0}	1.71×10^{0}	2.02×10^{0}
	3.16×10^{0}	2.31×10^{0}	1.83×10^{0}	1.73×10^{0}	1.76×10^{0}	2.04×10^{0}
3p–4p	4.96×10^{0}	4.69×10^{0}	4.57×10^{0}	4.67×10^{0}	4.85×10^{0}	5.47×10^{0}
	5.46×10^{0}	5.21×10^{0}	5.17×10^{0}	5.35×10^{0}	5.59×10^{0}	6.35×10^{0}
	5.85×10^{0}	5.67×10^{0}	5.76×10^{0}	6.01×10^{0}	6.28×10^{0}	7.06×10^{0}
3p–4d	6.86×10^{0}	7.04×10^{0}	7.53×10^{0}	8.29×10^{0}	9.19×10^{0}	1.23×10^{1}
	7.50×10^{0}	7.64×10^{0}	8.06×10^{0}	8.79×10^{0}	9.66×10^{0}	1.27×10^{1}
	7.49×10^{0}	7.69×10^{0}	8.27×10^{0}	9.06×10^{0}	9.96×10^{0}	1.30×10^{1}
3p–4f	7.12×10^{0}	7.47×10^{0}	7.98×10^{0}	8.60×10^{0}	9.24×10^{0}	1.11×10^{1}
	7.85×10^{0}	8.23×10^{0}	8.78×10^{0}	9.42×10^{0}	1.01×10^{1}	1.19×10^{1}
	8.42×10^{0}	8.77×10^{0}	9.35×10^{0}	9.98×10^{0}	1.06×10^{1}	1.23×10^{1}
3d–4s	6.40×10^{0}	3.92×10^{0}	2.37×10^{0}	1.79×10^{0}	1.49×10^{0}	1.04×10^{0}
	4.62×10^{0}	3.03×10^{0}	1.96×10^{0}	1.55×10^{0}	1.33×10^{0}	9.87×10^{-1}
	4.82×10^{0}	3.08×10^{0}	1.95×10^{0}	1.52×10^{0}	1.29×10^{0}	9.37×10^{-1}
3d–4p	5.89×10^{0}	4.64×10^{0}	3.59×10^{0}	3.11×10^{0}	2.85×10^{0}	2.43×10^{0}
	6.40×10^{0}	5.15×10^{0}	4.03×10^{0}	3.51×10^{0}	3.22×10^{0}	2.72×10^{0}
	6.35×10^{0}	5.01×10^{0}	3.96×10^{0}	3.48×10^{0}	3.19×10^{0}	2.68×10^{0}
3d–4d	1.02×10^{1}	9.78×10^{0}	9.12×10^{0}	8.93×10^{0}	8.94×10^{0}	9.33×10^{0}
	1.14×10^{1}	1.10×10^{1}	1.05×10^{1}	1.04×10^{1}	1.06×10^{1}	1.12×10^{1}
	1.17×10^{1}	1.15×10^{1}	1.13×10^{1}	1.14×10^{1}	1.17×10^{1}	1.23×10^{1}
3d–4f	3.41×10^{1}	3.57×10^{1}	3.90×10^{1}	4.31×10^{1}	4.76×10^{1}	6.17×10^{1}
	3.64×10^{1}	3.86×10^{1}	4.25×10^{1}	4.69×10^{1}	5.14×10^{1}	6.53×10^{1}
	4.05×10^{1}	4.23×10^{1}	4.58×10^{1}	4.97×10^{1}	5.39×10^{1}	6.71×10^{1}
4s–4p	1.43×10^{2}	1.59×10^{2}	1.83×10^{2}	2.07×10^{2}	2.30×10^{2}	2.93×10^{2}
	1.47×10^{2}	1.66×10^{2}	1.96×10^{2}	2.22×10^{2}	2.46×10^{2}	3.09×10^{2}
	1.40×10^{2}	1.60×10^{2}	1.91×10^{2}	2.19×10^{2}	2.43×10^{2}	3.07×10^{2}
4s–4d	3.21×10^{1}	3.07×10^{1}	2.90×10^{1}	2.85×10^{1}	2.84×10^{1}	2.87×10^{1}
	3.67×10^{1}	3.52×10^{1}	3.34×10^{1}	3.28×10^{1}	3.26×10^{1}	3.23×10^{1}
	3.51×10^{1}	3.43×10^{1}	3.31×10^{1}	3.26×10^{1}	3.25×10^{1}	3.22×10^{1}

Table 2. (Continued)

	Electron temperature (K)					
Transition	2.25×10^4	4.50×10^4	9.00×10^4	1.35×10^5	1.80×10^5	3.60×10^5
4s–4f	7.32×10^0	6.55×10^0	5.55×10^0	5.05×10^0	4.78×10^0	4.35×10^0
	8.72×10^0	7.63×10^0	6.32×10^0	5.67×10^0	5.30×10^0	4.64×10^0
	6.39×10^0	5.83×10^0	5.19×10^0	4.88×10^0	4.71×10^0	4.39×10^0
4p–4d	3.28×10^2	3.78×10^2	4.65×10^2	5.43×10^2	6.10×10^2	7.85×10^2
	4.44×10^2	5.09×10^2	5.90×10^2	6.55×10^2	7.11×10^2	8.55×10^2
	4.55×10^2	5.20×10^2	6.02×10^2	6.68×10^2	7.24×10^2	8.68×10^2
4p–4f	4.52×10^1	4.19×10^1	3.79×10^1	3.61×10^1	3.52×10^1	3.37×10^1
	4.84×10^1	4.47×10^1	4.00×10^1	3.77×10^1	3.64×10^1	3.41×10^1
	4.42×10^1	4.07×10^1	3.82×10^1	3.68×10^1	3.59×10^1	3.37×10^1
4d–4f	7.75×10^2	9.26×10^2	1.09×10^3	1.20×10^3	1.29×10^3	1.51×10^3
	9.18×10^2	1.07×10^3	1.22×10^3	1.31×10^3	1.39×10^3	1.57×10^3
	8.98×10^2	1.06×10^3	1.21×10^3	1.31×10^3	1.39×10^3	1.58×10^3

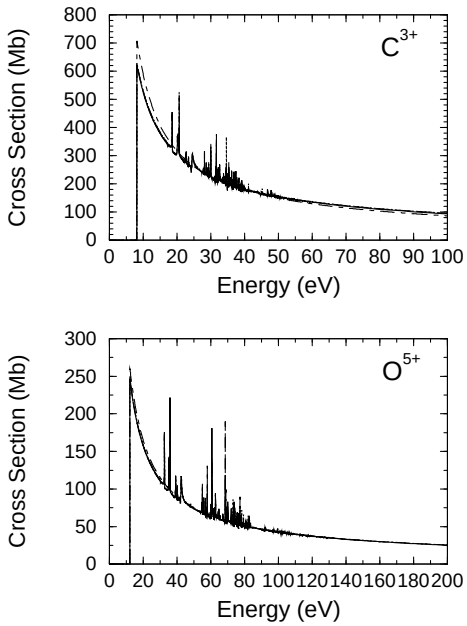

Figure 2. Electron-impact excitation cross sections for the 2s $\rightarrow$ 2p transition in C^{3+} and O^{5+}. The dotted, dashed, and solid curves (nearly indistinguishable in the graphs) are from the present 9-state non-pseudo-state *R*-matrix calculations, the 13-state non-pseudo-state *R*-matrix calculations, and the present 41-state RMPS calculations, respectively; the dot-dashed curves are calculated from the fitting formula of Fisher *et al* [7].

our non-pseudo-state *R*-matrix and RMPS calculations in comparison to the cross sections calculated from the fitting formula of Fisher *et al* [7] over an extended energy range. As can be seen, the cross sections for both ions from our calculations are impossible to distinguish on the scale of these graphs. Furthermore, the cross sections obtained from the formula of Fisher *et al* [7] appear to be in reasonably good agreement with our non-pseudo-state *R*-matrix and RMPS cross sections, especially for O^{5+}; however, for C^{3+}, the cross section from this formula is somewhat high near threshold and a little low at high energies.

The differences between the three sets of effective collision strengths for the other excitations shown in tables 1 and 2 for C^{3+} and in tables 3 and 4 for O^{5+} are in general much larger. With the exception of the 2s $\rightarrow$ 4f transition in O^{5+}, the RMPS effective collision strengths (first row) are smaller than the 9-state effective collision strengths (third

Table 3. Effective collision strengths for the first 18 transitions between the lowest nine terms of O^{5+}. For each transition, the first row is from the present 41-state pseudo-state calculation, the second row is from the present 13-state calculation, and the third row is from the present 9-state calculation.

	Electron temperature (K)					
Transition	5.00×10^4	1.00×10^5	2.00×10^5	3.00×10^5	4.00×10^5	8.00×10^5
2s–2p	5.09×10^0	5.26×10^0	5.56×10^0	5.79×10^0	6.00×10^0	6.59×10^0
	5.12×10^0	5.29×10^0	5.59×10^0	5.82×10^0	6.04×10^0	6.64×10^0
	5.13×10^0	5.30×10^0	5.59×10^0	5.83×10^0	6.04×10^0	6.64×10^0
2s–3s	2.65×10^{-1}	2.26×10^{-1}	1.98×10^{-1}	1.87×10^{-1}	1.82×10^{-1}	1.77×10^{-1}
	2.61×10^{-1}	2.27×10^{-1}	2.04×10^{-1}	1.95×10^{-1}	1.91×10^{-1}	1.90×10^{-1}
	2.70×10^{-1}	2.35×10^{-1}	2.11×10^{-1}	2.01×10^{-1}	1.97×10^{-1}	1.94×10^{-1}
2s–3p	1.52×10^{-1}	1.44×10^{-1}	1.38×10^{-1}	1.37×10^{-1}	1.40×10^{-1}	1.58×10^{-1}
	1.69×10^{-1}	1.56×10^{-1}	1.48×10^{-1}	1.46×10^{-1}	1.47×10^{-1}	1.64×10^{-1}
	1.65×10^{-1}	1.58×10^{-1}	1.52×10^{-1}	1.50×10^{-1}	1.51×10^{-1}	1.67×10^{-1}
2s–3d	2.57×10^{-1}	2.69×10^{-1}	2.76×10^{-1}	2.80×10^{-1}	2.86×10^{-1}	3.14×10^{-1}
	2.73×10^{-1}	2.89×10^{-1}	3.00×10^{-1}	3.07×10^{-1}	3.15×10^{-1}	3.45×10^{-1}
	2.85×10^{-1}	3.04×10^{-1}	3.16×10^{-1}	3.22×10^{-1}	3.29×10^{-1}	3.56×10^{-1}
2s–4s	4.37×10^{-2}	3.76×10^{-2}	3.32×10^{-2}	3.18×10^{-2}	3.13×10^{-2}	3.13×10^{-2}
	5.17×10^{-2}	4.46×10^{-2}	3.96×10^{-2}	3.80×10^{-2}	3.75×10^{-2}	3.76×10^{-2}
	5.88×10^{-2}	4.86×10^{-2}	4.25×10^{-2}	4.07×10^{-2}	4.01×10^{-2}	3.98×10^{-2}
2s–4p	5.63×10^{-2}	4.99×10^{-2}	4.38×10^{-2}	4.17×10^{-2}	4.12×10^{-2}	4.34×10^{-2}
	6.83×10^{-2}	6.02×10^{-2}	5.30×10^{-2}	5.06×10^{-2}	4.99×10^{-2}	5.14×10^{-2}
	6.00×10^{-2}	5.55×10^{-2}	5.19×10^{-2}	5.11×10^{-2}	5.13×10^{-2}	5.40×10^{-2}
2s–4d	6.49×10^{-2}	6.09×10^{-2}	5.61×10^{-2}	5.45×10^{-2}	5.43×10^{-2}	5.65×10^{-2}
	8.42×10^{-2}	7.76×10^{-2}	7.20×10^{-2}	7.07×10^{-2}	7.07×10^{-2}	7.28×10^{-2}
	7.00×10^{-2}	7.02×10^{-2}	7.02×10^{-2}	7.12×10^{-2}	7.23×10^{-2}	7.59×10^{-2}
2s–4f	4.51×10^{-2}	4.14×10^{-2}	3.64×10^{-2}	3.41×10^{-2}	3.29×10^{-2}	3.15×10^{-2}
	5.46×10^{-2}	4.89×10^{-2}	4.26×10^{-2}	3.98×10^{-2}	3.82×10^{-2}	3.55×10^{-2}
	4.07×10^{-2}	3.90×10^{-2}	3.67×10^{-2}	3.57×10^{-2}	3.51×10^{-2}	3.40×10^{-2}
2p–3s	6.46×10^{-1}	4.40×10^{-1}	2.95×10^{-1}	2.37×10^{-1}	2.05×10^{-1}	1.59×10^{-1}
	6.04×10^{-1}	4.26×10^{-1}	2.94×10^{-1}	2.38×10^{-1}	2.09×10^{-1}	1.63×10^{-1}
	6.27×10^{-1}	4.43×10^{-1}	3.05×10^{-1}	2.47×10^{-1}	2.15×10^{-1}	1.67×10^{-1}
2p-3p	1.16×10^0	9.87×10^{-1}	8.71×10^{-1}	8.16×10^{-1}	7.84×10^{-1}	7.39×10^{-1}
	1.07×10^0	9.76×10^{-1}	9.02×10^{-1}	8.62×10^{-1}	8.39×10^{-1}	8.06×10^{-1}
	1.07×10^0	9.97×10^{-1}	9.32×10^{-1}	8.92×10^{-1}	8.67×10^{-1}	8.28×10^{-1}
2p–3d	2.32×10^0	2.36×10^0	2.40×10^0	2.45×10^0	2.53×10^0	2.86×10^0
	2.43×10^0	2.48×10^0	2.54×10^0	2.60×10^0	2.69×10^0	3.04×10^0
	2.49×10^0	2.55×10^0	2.62×10^0	2.68×10^0	2.77×10^0	3.11×10^0
2p–4s	9.62×10^{-2}	7.35×10^{-2}	5.52×10^{-2}	4.69×10^{-2}	4.22×10^{-2}	3.41×10^{-2}
	1.18×10^{-1}	8.88×10^{-2}	6.62×10^{-2}	5.62×10^{-2}	5.04×10^{-2}	4.00×10^{-2}
	1.30×10^{-1}	9.24×10^{-2}	6.74×10^{-2}	5.72×10^{-2}	5.13×10^{-2}	4.10×10^{-2}
2p–4p	2.55×10^{-1}	2.26×10^{-1}	1.93×10^{-1}	1.78×10^{-1}	1.69×10^{-1}	1.55×10^{-1}
	3.38×10^{-1}	2.89×10^{-1}	2.44×10^{-1}	2.24×10^{-1}	2.12×10^{-1}	1.92×10^{-1}
	2.64×10^{-1}	2.44×10^{-1}	2.22×10^{-1}	2.12×10^{-1}	2.06×10^{-1}	1.92×10^{-1}
2p–4d	4.83×10^{-1}	4.65×10^{-1}	4.45×10^{-1}	4.46×10^{-1}	4.55×10^{-1}	5.02×10^{-1}
	5.88×10^{-1}	5.64×10^{-1}	5.45×10^{-1}	5.50×10^{-1}	5.61×10^{-1}	6.08×10^{-1}
	5.39×10^{-1}	5.43×10^{-1}	5.49×10^{-1}	5.64×10^{-1}	5.80×10^{-1}	6.32×10^{-1}
2p–4f	2.47×10^{-1}	2.22×10^{-1}	1.88×10^{-1}	1.72×10^{-1}	1.63×10^{-1}	1.50×10^{-1}
	2.88×10^{-1}	2.52×10^{-1}	2.11×10^{-1}	1.92×10^{-1}	1.81×10^{-1}	1.63×10^{-1}
	1.92×10^{-1}	1.80×10^{-1}	1.64×10^{-1}	1.57×10^{-1}	1.53×10^{-1}	1.47×10^{-1}

Table 3. (Continued)

	Electron temperature (K)					
Transition	5.00×10^4	1.00×10^5	2.00×10^5	3.00×10^5	4.00×10^5	8.00×10^5
3s–3p	3.13×10^1	3.34×10^1	3.61×10^1	3.82×10^1	4.02×10^1	4.62×10^1
	3.07×10^1	3.27×10^1	3.55×10^1	3.78×10^1	3.98×10^1	4.61×10^1
	3.07×10^1	3.28×10^1	3.56×10^1	3.79×10^1	4.00×10^1	4.62×10^1
3s–3d	4.06×10^0	3.86×10^0	3.60×10^0	3.42×10^0	3.32×10^0	3.13×10^0
	4.13×10^0	3.94×10^0	3.68×10^0	3.51×10^0	3.40×10^0	3.21×10^0
	4.20×10^0	4.05×10^0	3.80×10^0	3.62×10^0	3.50×10^0	3.28×10^0
3s–4s	9.87×10^{-1}	8.61×10^{-1}	7.89×10^{-1}	7.78×10^{-1}	7.84×10^{-1}	8.24×10^{-1}
	9.68×10^{-1}	8.81×10^{-1}	8.36×10^{-1}	8.39×10^{-1}	8.54×10^{-1}	9.07×10^{-1}
	9.83×10^{-1}	9.11×10^{-1}	8.78×10^{-1}	8.85×10^{-1}	9.00×10^{-1}	9.50×10^{-1}

row) for excitations from the 2s ground state. This is what one would expect to result from coupling to the the target continuum states, as well as to the highly excited bound states, that is included in the RMPS calculations, but not the 9-state calculation. However, this comparison of the RMPS and 9-state effective collision strengths is somewhat misleading, especially for excitation to the terms of the 4ℓ configurations. The comparisons with the 9-state calculations were included here primarily because previous comparisons in Be^+ [3] and B^{2+} [4] had been made between RMPS and non-pseudo-state 9-state R-matrix calculations. However, if one is interested in obtaining more accurate results for excitation to the 4ℓ terms of these ions from non-pseudo-state calculations, the 5ℓ terms should be part of the close-coupling expansions; in this way, one can include both coupling to the $n = 5$ terms (that will tend to lower the effective collision strengths) and resonance contributions from those terms (that will increase the effective collision strengths).

Thus, comparisons of the RMPS and 13-state collision strengths shown in the first two rows for each transition in tables 1 and 2 for C^{3+} and tables 3 and 4 for O^{5+} are more meaningful than comparisons between the RMPS and 9-state collision strengths, particularly for transitions to the 4ℓ terms. This is especially true because the 5ℓ states generated from the Laguerre basis in our RMPS calculations provide a good representation of the 5ℓ spectroscopic states included in our 13-state non-pseudo-state R-matrix calculations. For example, in O^{5+}, we found that the 5ℓ pseudo-state energies were, on average, only 0.33 eV or 0.28% high as compared with the 5ℓ HF energies. Furthermore, the dipole line strengths to the 5ℓ pseudo-states were, on average, only 11% high as compared with the dipole line strengths to 5ℓ HF states. This agreement between the 5ℓ pseudo-states and the 5ℓ HF states is consistent with extensive CCC calculations, where it has been found that the low-lying bound pseudo-states, calculated from a set of orthogonal Laguerre pseudo-orbitals, quickly converge to the physical states as the size of the basis set is increased [20].

Thus we would expect that the 13-state and the RMPS calculations of the contributions to excitation arising from resonances attached to the terms of the 5ℓ configuration should be in reasonably good agreement and that the differences between the results of these two calculations should be due primarily to coupling to the target continuum included in the RMPS calculation. This is illustrated in figure 3 where we compare the 9-state non-pseudo-state R-matrix, the 13-state non-pseudo-state R-matrix and the RMPS cross sections for the $2s \rightarrow 4f$ excitation in O^{5+} in the resonance region. Of course, no resonance contributions arise from the 9-state calculation, but as one would expect, it has a larger background cross section than that resulting from either the 13-state or the RMPS calculations. On the other hand, the larger resonance structures in the 13-state and the RMPS cross sections are quite similar, although

Table 4. Effective collision strengths for the last 18 transitions between the lowest nine terms of O^{5+}. For each transition, the first row is from the present 41-state pseudo-state calculation, the second row is from the present 13-state calculation, and the third row is from the present 9-state calculation.

	Electron temperature (K)					
Transition	5.00×10^4	1.00×10^5	2.00×10^5	3.00×10^5	4.00×10^5	8.00×10^5
3s–4p	4.32×10^{-1}	3.98×10^{-1}	3.89×10^{-1}	4.13×10^{-1}	4.48×10^{-1}	5.94×10^{-1}
	4.83×10^{-1}	4.24×10^{-1}	4.01×10^{-1}	4.20×10^{-1}	4.52×10^{-1}	5.91×10^{-1}
	3.74×10^{-1}	3.57×10^{-1}	3.66×10^{-1}	3.98×10^{-1}	4.37×10^{-1}	5.86×10^{-1}
3s–4d	7.62×10^{-1}	7.61×10^{-1}	7.74×10^{-1}	8.09×10^{-1}	8.49×10^{-1}	9.77×10^{-1}
	8.24×10^{-1}	8.09×10^{-1}	8.11×10^{-1}	8.43×10^{-1}	8.80×10^{-1}	1.00×10^{0}
	7.18×10^{-1}	7.36×10^{-1}	7.75×10^{-1}	8.23×10^{-1}	8.69×10^{-1}	1.00×10^{0}
3s–4f	1.01×10^{0}	9.87×10^{-1}	9.55×10^{-1}	9.54×10^{-1}	9.62×10^{-1}	9.93×10^{-1}
	1.12×10^{0}	1.09×10^{0}	1.05×10^{0}	1.04×10^{0}	1.04×10^{0}	1.05×10^{0}
	1.08×10^{0}	1.07×10^{0}	1.04×10^{0}	1.04×10^{0}	1.05×10^{0}	1.06×10^{0}
3p–3d	6.08×10^{1}	6.34×10^{1}	6.79×10^{1}	7.21×10^{1}	7.61×10^{1}	8.83×10^{1}
	6.50×10^{1}	6.94×10^{1}	7.47×10^{1}	7.87×10^{1}	8.23×10^{1}	9.28×10^{1}
	6.54×10^{1}	6.99×10^{1}	7.52×10^{1}	7.92×10^{1}	8.27×10^{1}	9.32×10^{1}
3p–4s	1.10×10^{0}	8.01×10^{-1}	6.36×10^{-1}	6.03×10^{-1}	6.10×10^{-1}	7.09×10^{-1}
	1.06×10^{0}	7.84×10^{-1}	6.32×10^{-1}	6.03×10^{-1}	6.11×10^{-1}	7.06×10^{-1}
	1.00×10^{0}	7.41×10^{-1}	6.06×10^{-1}	5.85×10^{-1}	5.96×10^{-1}	6.95×10^{-1}
3p–4p	2.73×10^{0}	2.60×10^{0}	2.52×10^{0}	2.56×10^{0}	2.62×10^{0}	2.86×10^{0}
	3.06×10^{0}	2.87×10^{0}	2.80×10^{0}	2.85×10^{0}	2.93×10^{0}	3.20×10^{0}
	2.90×10^{0}	2.85×10^{0}	2.88×10^{0}	2.97×10^{0}	3.07×10^{0}	3.36×10^{0}
3p–4d	3.95×10^{0}	3.98×10^{0}	4.17×10^{0}	4.54×10^{0}	4.95×10^{0}	6.39×10^{0}
	4.25×10^{0}	4.20×10^{0}	4.36×10^{0}	4.71×10^{0}	5.11×10^{0}	6.52×10^{0}
	3.84×10^{0}	3.95×10^{0}	4.26×10^{0}	4.67×10^{0}	5.10×10^{0}	6.55×10^{0}
3p–4f	4.19×10^{0}	4.22×10^{0}	4.30×10^{0}	4.50×10^{0}	4.72×10^{0}	5.40×10^{0}
	4.62×10^{0}	4.56×10^{0}	4.60×10^{0}	4.78×10^{0}	4.99×10^{0}	5.63×10^{0}
	4.30×10^{0}	4.38×10^{0}	4.56×10^{0}	4.79×10^{0}	5.03×10^{0}	5.70×10^{0}
3d–4s	1.84×10^{0}	1.16×10^{0}	7.35×10^{-1}	5.70×10^{-1}	4.84×10^{-1}	3.50×10^{-1}
	1.63×10^{0}	1.05×10^{0}	6.74×10^{-1}	5.30×10^{-1}	4.53×10^{-1}	3.33×10^{-1}
	1.26×10^{0}	8.02×10^{-1}	5.25×10^{-1}	4.22×10^{-1}	3.69×10^{-1}	2.86×10^{-1}
3d–4p	2.05×10^{0}	1.73×10^{0}	1.38×10^{0}	1.21×10^{0}	1.11×10^{0}	9.54×10^{-1}
	2.59×10^{0}	2.06×10^{0}	1.58×10^{0}	1.36×10^{0}	1.23×10^{0}	1.02×10^{0}
	1.67×10^{0}	1.42×10^{0}	1.19×10^{0}	1.08×10^{0}	1.01×10^{0}	9.04×10^{-1}
3d–4d	5.81×10^{0}	5.46×10^{0}	4.99×10^{0}	4.82×10^{0}	4.76×10^{0}	4.81×10^{0}
	6.58×10^{0}	6.09×10^{0}	5.58×10^{0}	5.42×10^{0}	5.38×10^{0}	5.43×10^{0}
	5.51×10^{0}	5.39×10^{0}	5.27×10^{0}	5.29×10^{0}	5.34×10^{0}	5.51×10^{0}
3d–4f	1.99×10^{1}	2.04×10^{1}	2.15×10^{1}	2.32×10^{1}	2.50×10^{1}	3.07×10^{1}
	2.14×10^{1}	2.18×10^{1}	2.29×10^{1}	2.45×10^{1}	2.62×10^{1}	3.18×10^{1}
	2.14×10^{1}	2.19×10^{1}	2.32×10^{1}	2.48×10^{1}	2.65×10^{1}	3.20×10^{1}
4s–4p	9.73×10^{1}	1.02×10^{2}	1.12×10^{2}	1.23×10^{2}	1.34×10^{2}	1.64×10^{2}
	1.00×10^{2}	1.08×10^{2}	1.21×10^{2}	1.33×10^{2}	1.44×10^{2}	1.72×10^{2}
	1.01×10^{2}	1.10×10^{2}	1.23×10^{2}	1.36×10^{2}	1.46×10^{2}	1.74×10^{2}
4s–4d	1.48×10^{1}	1.42×10^{1}	1.34×10^{1}	1.31×10^{1}	1.31×10^{1}	1.30×10^{1}
	1.55×10^{1}	1.50×10^{1}	1.42×10^{1}	1.39×10^{1}	1.38×10^{1}	1.36×10^{1}
	1.59×10^{1}	1.54×10^{1}	1.46×10^{1}	1.44×10^{1}	1.42×10^{1}	1.40×10^{1}
4s–4f	3.06×10^{0}	2.75×10^{0}	2.32×10^{0}	2.11×10^{0}	1.99×10^{0}	1.80×10^{0}
	3.24×10^{0}	2.82×10^{0}	2.35×10^{0}	2.13×10^{0}	2.01×10^{0}	1.81×10^{0}
	2.21×10^{0}	2.04×10^{0}	1.85×10^{0}	1.77×10^{0}	1.72×10^{0}	1.66×10^{0}

Table 4. (Continued)

	Electron temperature (K)					
Transition	5.00×10^4	1.00×10^5	2.00×10^5	3.00×10^5	4.00×10^5	8.00×10^5
4p–4d	1.77×10^2	2.00×10^2	2.41×10^2	2.77×10^2	3.08×10^2	3.86×10^2
	2.56×10^2	2.79×10^2	3.11×10^2	3.38×10^2	3.61×10^2	4.21×10^2
	2.56×10^2	2.79×10^2	3.12×10^2	3.40×10^2	3.64×10^2	4.24×10^2
4p–4f	2.07×10^1	1.92×10^1	1.72×10^1	1.62×10^1	1.57×10^1	1.47×10^1
	2.21×10^1	2.01×10^1	1.78×10^1	1.67×10^1	1.61×10^1	1.50×10^1
	1.83×10^1	1.72×10^1	1.60×10^1	1.54×10^1	1.50×10^1	1.44×10^1
4d–4f	3.69×10^2	4.30×10^2	4.99×10^2	5.49×10^2	5.88×10^2	6.80×10^2
	4.47×10^2	5.06×10^2	5.62×10^2	6.03×10^2	6.35×10^2	7.10×10^2
	4.26×10^2	4.89×10^2	5.51×10^2	5.95×10^2	6.29×10^2	7.07×10^2

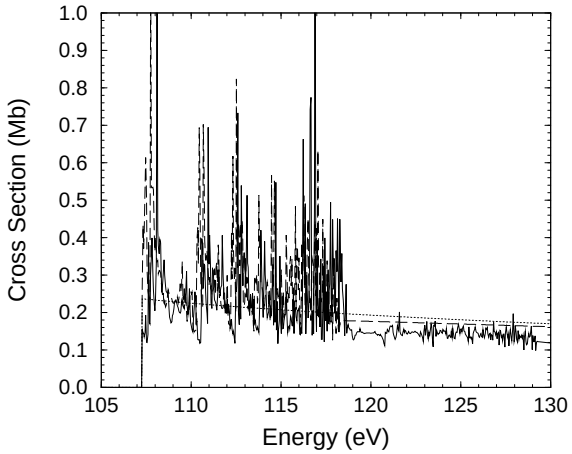

Figure 3. Electron-impact excitation cross sections for the 2s $\rightarrow$ 4f transition in O^{5+} in the resonance region. The dotted curve is from the present 9-state non-pseudo-state *R*-matrix calculation, the dashed curve is from the present 13-state non-pseudo-state *R*-matrix calculation, and the solid curve is from the present 41-state RMPS calculation.

those determined from the RMPS calculation are shifted to slightly higher energy because of the higher energies of the 5ℓ terms in the RMPS close-coupling expansion; there are also some differences in the size of some of the narrow resonances. The smaller resonance structures at higher energy seen in the RMPS cross section, and not in the 13-state cross section, are due to resonances attached to the 6ℓ states included in the RMPS calculation; they should provide at least some estimate for the relatively small resonance contributions from the more highly excited bound states. Therefore, unlike the 9-state 2s $\rightarrow$ 4f effective collision strengths given in table 3, the 13-state effective collision strengths for this transition are above the RMPS effective collision strengths due to the coupling to the target continuum included in the RMPS calculation.

For the vast majority of the transitions shown in tables 1 and 2 and tables 3 and 4, the RMPS effective effective collision strengths are below the 13-state effective collision strengths due to the coupling to the target continuum included in the RMPS calculation. The exceptions are the 2p $\rightarrow$ 3p, 3s $\rightarrow$ 3p, 3s $\rightarrow$ 4s, 3p $\rightarrow$ 4s and 3d $\rightarrow$ 4s excitations in both C^{3+} and O^{5+} and the 2p $\rightarrow$ 3s excitation in C^{3+}. Most of the differences for these transitions are relatively small and are due primarily to differences in the two calculations with respect to the resonant states attached to the upper 3ℓ and 4ℓ terms, rather than differences in the background.

To simplify these comparisons, we present temperature-averaged percentage differences between the RMPS and the 9-state effective collision strengths and between the RMPS and

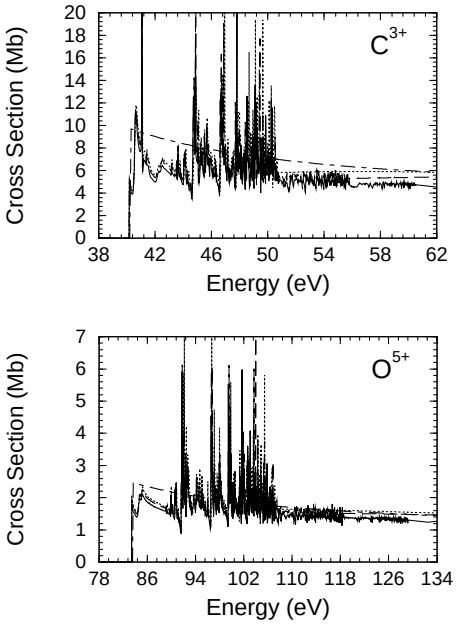

Figure 4. Electron-impact excitation cross sections for the 2s $\rightarrow$ 3d transition in C^{3+} and O^{5+}. The dotted curves are from the present 9-state non-pseudo-state *R*-matrix calculations; the dashed curves are from the present 13-state non-pseudo-state *R*-matrix calculations; the solid curves are from the present 41-state RMPS calculations; and the dot-dashed curves are from the fitting formula of Fisher *et al* [7].

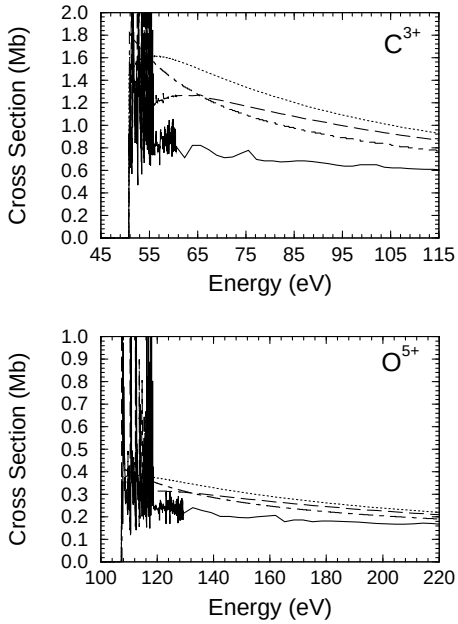

Figure 5. Electron-impact excitation cross sections for the 2s $\rightarrow$ 4d transition in C^{3+} and O^{5+}. The dotted curves are from the present 9-state non-pseudo-state *R*-matrix calculations; the dashed curves are from the present 13-state non-pseudo-state *R*-matrix calculations; the solid curves are from the present 41-state RMPS calculations; and the dot-dashed curves are from the fitting formula of Fisher *et al* [7].

13-state effective collision strengths for C^{3+} and O^{5+} in table 5, organized by the general type of the transition. As one might expect, this table indicates that the effects of coupling to the target continuum are relatively small for excitations to the terms of the 3ℓ configurations. However, they are quite large for the $2\ell \rightarrow 4\ell'$ transitions; if we concentrate on the comparisons between the RMPS and 13-state results for these transitions, we see that there is a significant reduction in these effects with ionization stage only for excitations to the terms of the 4d and 4f configurations, and even then they remain relatively large. It may seem surprising to find this large an effect, even for excitations to the terms of the 4ℓ configurations, in both three times and five times ionized species; however, these results are consistent with what was found regarding the 2s $\rightarrow$ 4ℓ cross sections in Be^{+} and B^{2+} [3, 4]. There is a wide range of temperature-averaged percentage differences for the $3\ell \rightarrow 4\ell'$ and $4\ell \rightarrow 4\ell'$ excitations; thus, it is difficult to make any general statement regarding the magnitude of the extra coupling effects for transitions between these more highly excited terms.

Finally, in figures 4 and 5, we present cross sections for the 2s $\rightarrow$ 3d and 2s $\rightarrow$ 4d excitations resulting from our RMPS calculations and our 13-state and 9-state non-pseudo-state *R*-matrix calculations in both C^{3+} and O^{5+}; also included in these graphs are the cross sections for these transitions determined from the fitting formula of Fisher *et al* [7]. These two transitions were selected to further illustrate important points regarding coupling to the target continuum states, as well as the resonance contributions to the cross sections.

Table 5. Temperature-averaged percentage differences between the effective collision strengths determined from the present calculations in C^{3+} and O^{5+}.

Transition	41-state and 9-state in C^{3+}	41-state and 13-state in C^{3+}	41-state and 9-state in O^{5+}	41-state and 13-state in O^{5+}
2s–2p	1.0	0.9	0.7	0.6
2s–3s	12.8	9.1	6.1	3.5
2s–3p	8.3	4.1	8.2	6.8
2s–3d	14.0	9.2	12.8	8.3
2p–3s	9.5	6.3	3.5	2.5
2p–3p	11.5	6.9	7.7	5.6
2p–3d	9.9	6.3	8.3	5.6
2s–4s	31.6	24.0	25.4	17.6
2s–4p	41.5	22.3	16.3	18.7
2s–4d	61.6	56.5	21.4	25.4
2s–4f	18.8	26.3	6.0	15.6
2p–4s	27.7	14.8	21.7	18.2
2p–4p	35.6	24.0	13.9	23.8
2p–4d	39.9	29.0	19.6	20.0
2p–4f	9.1	19.1	12.8	11.6
3s–3p	1.9	2.1	1.1	1.3
3s–3d	4.3	1.5	4.9	2.2
3p–3d	5.1	4.5	8.4	7.8
3s–4s	18.9	5.7	9.6	6.0
3s–4p	8.5	9.2	6.5	3.9
3s–4d	6.3	6.5	2.6	4.8
3s–4f	18.8	12.7	7.9	8.6
3p–4s	6.5	8.5	4.9	1.2
3p–4p	22.4	12.5	12.5	10.8
3p–4d	8.2	6.3	2.3	4.3
3p–4f	14.6	9.0	5.0	6.7
3d–4s	18.8	18.0	30.7	8.3
3d–4p	9.5	10.9	8.8	13.8
3d–4d	21.6	14.5	7.7	11.8
3d–4f	14.2	7.5	6.4	5.6
4s–4p	3.8	5.5	7.5	6.0
4s–4d	11.9	13.5	8.1	5.3
4s–4f	6.3	12.3	20.8	2.0
4p–4d	22.9	21.0	23.6	23.2
4p–4f	2.8	4.6	7.0	3.7
4d–4f	9.9	10.5	9.3	11.4

The cross section for the 2s $\rightarrow$ 3d excitation is shown in figure 4. We see in this case that the reduction in the background cross section due to the extra coupling contained within the RMPS calculations is relatively small in both ions, but clearly decreases with ionization stage. Furthermore, the large resonance structures from our three calculations are similar, although there are some differences in the very narrow resonances. The two groups of small narrow resonant structures present in the RMPS cross section are due to resonances attached to the 5ℓ and 6ℓ terms; they are of course absent in the 9-state cross sections, but the resonances attached to the 5ℓ terms from the 13-state cross sections are similar to those orginating from

the RMPS calculation. The cross sections determined from the formula due to Fisher *et al* are above *R*-matrix and RMPS cross sections but converge to the *R*-matrix cross sections at higher energy; furthermore, effective collision strengths determined from this formula would be in relatively good agreement with those given in tables 1 and 3 for this transition.

The situation is quite different for the 2s $\rightarrow$ 4d excitation shown in figure 5. In C^{3+}, the relatively large difference between the 9-state and the 13-state background cross sections is due to the coupling to the 5ℓ terms included in the 13-state calculation. The even larger difference between the 13-state and RMPS background cross section indicates the significance of coupling to the target continuum for this transition. Both of these effects decrease significantly with ionization stage, but are still far from negligible in O^{5+}. In the case of the 13-state and RMPS calculations, there are relatively large narrow resonances near threshold, arising from resonances attached to the $n = 5$ terms; the set of much smaller resonances appearing only in the RMPS cross sections at higher energy, arise from the resonances attached to the $n = 6$ terms. The small variations in the background cross sections at still higher energies, where we employ a coarser energy mesh, are due to resonances attached to pseudo-states above the ionization limit; these are characteristic of all RMPS calculations and they decrease in magnitude with the size of the Laguerre basis set. In this case, the cross sections calculated from the formula of Fisher *et al* [7] fall below the two non-pseudo-state *R*-matrix calculations, but are still well above the RMPS cross section, especially for C^{3+}.

4. Conclusions

We have performed extensive pseudo-state and non-pseudo-state calculations of electron-impact excitation in C^{3+} and O^{5+}. We have found that the effects of coupling to the target continuum are minimal for the 2s $\rightarrow$ 2p excitation in these ions, and these effects on the $2\ell \rightarrow 3\ell'$ effective collision strengths, when averaged over temperature, are less than 10% in both C^{3+} and O^{5+}. They are also small for the $3\ell \rightarrow 3\ell'$ transitions in both ions. Thus a non-pseudo-state calculation for excitations up to the $n = 3$ shell in these ions should be sufficiently accurate for most applications. However, the situation regarding excitations to the $n = 4$ shell is another matter. For C^{3+}, errors up to the order of 50% can be expected for transitions of the type $2\ell \rightarrow 4\ell'$ from a calculation that does not include coupling to the continuum. In five times ionized species and above the situation is somewhat better; there, errors up to the order of 25% can be expected for excitations up to the $n = 4$ shell, which may be acceptable for many applications.

These calculations also indicate that a properly designed pseudo-state calculation will include reasonably accurate contributions to the effective collision strengths from resonances attached to highly excited states. Thus we expect that our RMPS calculations for the effective collision strengths for transitions between the lowest nine terms of these ions are of sufficient accuracy for nearly all applications. Our RMPS data for effective collision strengths, on a somewhat wider temperature range than that appearing in the present tables, along with energy levels and electric dipole radiative rates, are now available on the Internet at the Oak Ridge National Laboratory (ORNL) Controlled Fusion Atomic Date Center (CFADC): www-cfadc.phy.ornl.gov/data-and-codes.

These results, along with those of earlier pseudo-state calculations [3–5], also have implications regarding the accuracy of electron-impact excitation calculations in more complex species. With a few exceptions, such as the RMPS calculations of electron-impact excitation between the low-lying terms in neutral beryllium [21] and neutral boron [22], pseudo-state calculations have been largely restricted to simple systems involving one electron above a closed shell. However, there are a number of efforts now underway to generate electron-impact

excitation data in complex atoms and ions for applications to laboratory and astrophysical plasma research. In many cases, these calculations may include a large number of open-shell physical states, must have a relatively large R-matrix box to contain the bound orbitals, must include a large expansion of the box states to properly represent the $(N+1)$-electron continuum to sufficiently high energies and must often be done in intermediate coupling. To also include a large number of pseudo-states within such complex calculations would provide a severe challenge even for modern massively parallel computers. Thus the majority of calculated excitation rates to the more highly excited states in complex species will be limited in accuracy by the fact that they will not include coupling to the N-electron continuum. The size of the errors involved will, of course, depend on the ionization stage. However, the present calculations seem to indicate that, at least in the lower ionization stages, the accuracy of such calculations may be more limited than we often assume.

Acknowledgments

In this work, DCG was supported by a US DoE Grant (DE-FG02-96-ER54367) with Rollins College and MSP was supported by a US DoE Grant (DE-FG05-96-ER54348) with Auburn University.

References

[1] Bray I and Stelbovics A T 1992 *Phys. Rev. Lett.* **69** 53–6
[2] Bartschat K, Hudson E T, Scott M P, Burke P G and Burke V M 1996 *J. Phys. B: At. Mol. Opt. Phys.* **29** 115–23
[3] Bartschat K and Bray I 1997 *J. Phys. B: At. Mol. Opt. Phys.* **30** L109–14
[4] Marchalant P J, Bartschat K and Bray I 1997 *J. Phys. B: At. Mol. Opt. Phys.* **30** L435–40
[5] Badnell N R and Gorczyca T W 1997 *J. Phys. B: At. Mol. Opt. Phys.* **30** 2011–9
[6] Burke V M 1992 *J. Phys. B: At. Mol. Opt. Phys.* **25** 4917–28
[7] Fisher V I, Ralchenko Y V, Bernshtam V A, Goldgirsh A, Maron Y, Vainshtein L A and Bray I 1997 *Phys. Rev.* A **56** 3726–33
[8] Janzen P H, Gardner L D, Reisenfeld D B, Savin D W, Kohl J L and Bartschat K 1999 *Phys. Rev.* A **59** 4821–4
[9] Mitnik D M, Pindzola M S, Griffin D C and Badnell N R 1999 *J. Phys. B: At. Mol. Opt. Phys.* **32** L479–85
[10] Froese Fischer C 1991 *Comput. Phys. Commun.* **64** 369–98
[11] Badnell N R 1986 *J. Phys. B: At. Mol. Phys.* **19** 3827–35
[12] Brillouin L 1932 *J. Phys. Radium* **3** 373
[13] Berrington K A, Eissner W B and Norrington P H 1995 *Comput. Phys. Commun.* **92** 290–420
[14] Gorczyca T W and Badnell N R 1997 *J. Phys. B: At. Mol. Opt. Phys.* **30** 3897–911
[15] Badnell N R, Pindzola M S, Bray I and Griffin D C 1999 *J. Phys. B: At. Mol. Opt. Phys.* **32** 911–24
[16] Seaton M J 1953 *Proc. R. Soc.* A **218** 400–16
[17] Taylor P O, Gregory D, Dunn G H, Phaneuf R A and Crandall D H 1977 *Phys. Rev. Lett.* **39** 1256–9
[18] Bannister M E, Chung Y S, Djuric N, Wallbank B, Woitke O, Zhou S, Dunn G H and Smith A C H 1998 *Phys. Rev.* A **57** 278–81
[19] Greenwood J B, Smith S J and Chutjian A 1999 *Phys. Rev.* A **59** 1348–54
[20] Bray I 1994 *Phys. Rev.* A **49** 1066–82
[21] Bartschat K, Burke P G and Scott M P 1996 *J. Phys. B: At. Mol. Opt. Phys.* **29** L769–72
[22] Marchalant P J, Bartschat K, Berrington K A and Nakazaki S 1997 *J. Phys. B: At. Mol. Opt. Phys.* **30** L279–83